Simulations of Air-assisted Primary Atomization at Different Air-to-Liquid Injection Angles for Entrained Flow Gasification

F. Zhang[1*], T. Zirwes[2,1], S. Wachter[3], T. Jakobs[3], P. Habisreuther[1],

N. Zarzalis[1], D. Trimis[1], T. Kolb[3], H. Bockhorn[1]

* feichi.zhang@kit.edu

[1]*Engler-Bunte-Institute/Division for Combustion Technology, Karlsruhe Institute of Technology, Engler-Bunte-Ring 7, 76131, Karlsruhe, Germany*
[2]*Steinbuch Centre for Computing, Karlsruhe Institute of Technology, Hermann-von-Helmholtz-Platz 1, 76344 Eggenstein-Leopoldshafen,Germany*
[3]*Institute for Technical Chemistry, Karlsruhe Institute of Technology, Hermann-von-Helmholtz-Platz 1, 76344 Eggenstein-Leopoldshafen, Germany*

Abstract
Highly-resolved numerical simulations have been performed for a coaxial, twin-fluid nozzle, which is designed for fundamental research of the atomization process in entrained flow gasification (EFG). Objective of the work is to reveal specifically the influence of the relative injection angle α between the central liquid jet and the annular airflow (external-mixing) on the primary atomization. A glycerol/water mixture with a dynamic viscosity of 200 mPa·s is atomized at atmospheric condition and with a gas-to-liquid ratio of 0.6. The angle of attack between liquid and airflow has been varied from α = 0° to 60°. The computational grid consists of approx. 10 million cells, using a smallest resolution of 25 µm. In agreement with the corresponding experiment, the calculated breakup morphology is characterized by a pulsating mode destabilization, accompanied by disintegration of membrane-type ligaments. The breakup of the liquid jet is found to be enhanced from α = 0° to 30°, which leads to a decrease of the liquid core length L_C. This is attributable to a reinforced aerodynamic interaction or an enhanced multiphase momentum transfer from the gas to the liquid phase, respectively. The gas flow velocity close to the liquid jet is increased in this case, which is in accordance with results obtained from the PIV measurement. The reason for the increase of local flow velocity is shown to be caused by an increased local static pressure at the base of the liquid jet with increased α, which results in a favorable pressure gradient in main flow direction. However, further increase of α from 30° to 60° leads to a decreased flow velocity around the liquid jet, so that L_C increases and the atomization performance decreases with α. The behavior is further elucidated by means of the multiphase momentum exchange or the liquid phase kinetic energy, which increase from α = 0° to 30° and decreases with further increased α. The result reveals the essential impact of the nozzle design parameters on the atomization process in addition to the general operating parameters. In summary, there exists an optimal relative injection angle between the liquid and air streams in the range of 30°<α<45° for a best atomization performance.

Introduction
Entrained flow gasification (EFG) is applied for the conversion of solid and liquid fuels to a synthesis gas, which is to be used to produce basic chemicals or liquid fuels [01-03]. In addition, it can be directly burnt for operating gas turbines in a combined cycle power plant with high energy efficiency. EFG is an enabling technology to reach the goals of the European Green Deal, as it converts biogenic as well as fossil based fuel into the chemical building blocks CO and H_2 and, thus, can make a substantial contribution to circular economy and reduction of greenhouse gas. Besides the complex gasification

reactions, an optimized atomization of liquid fuel in an EFG is of significant importance on the overall performance of the gasifier and the quality of the produced syngas [04, 05]. For example, it is particularly important to avoid large droplets, which may lead to incomplete evaporation due to the short residence time in the gasifier. On the other hand, a well-distributed spray of liquid fuel with small droplets can be evaporated efficiently, which improves performance of mixing and gasification of fuel vapor.

Gas-assisted nozzles are generally used for liquid fed EFG, where a low-speed liquid stream is subjected to aerodynamic strain from the high-speed ambient gas flow and is disintegrated into small droplets by means of momentum transfer from the gas phase. The primary breakup in the near-nozzle field is controlled by a competition between the cohesive and disruptive forces, which gives rise to oscillations and instabilities on the surface of the liquid fuel column. Under favorable conditions, the instabilities are amplified and the liquid jet column disintegrates into ligaments and droplets [04]. If the shear stress from the surrounding gas flow is high and the primary droplets exceed a critical size, they further break up into smaller droplets, a process known as secondary atomization. The primary breakup process is of particular importance for the formation of the final spray, which connects the initial deformation of the liquid jet core and the disintegration of primary liquid fragments [06]. Due to limited optical access of the near-nozzle flow field, previous experimental works on primary atomization were mainly focused on the morphology of the breakup process by means of high-speed imaging, from which some basic properties of the liquid jet can be developed as a function of the operating parameters [06-14]. As different nozzle geometries were applied in these works and the desired measurement quantities, such as the breakup length or frequency of the liquid jet, were difficult to distinguish for many test conditions, the available data and correlations are of questionable generality and the physics behind primary atomization is still not well understood. In addition, water was mostly used in the previous studies, whereas EFG commonly applies high viscous liquids, as well as suspension fuels with complex rheological behavior. The atomization process is further complicated, while the liquid jet is disturbed by the turbulent gas flow over a wide range of length and time scales [08]. So far, the physics of primary breakup in EFG have not been unveiled, as it is affected by a large number of operating and nozzle design parameters. It is additionally not sufficient to describe atomization performance solely by scalar geometrical and operational parameters, but the nozzle interior geometries and the injection direction of the atomizing fluids in relation to each other and to the ambient play an important role [14].

To overcome these difficulties and to gain a more detailed understanding of the fundamental mechanisms prevailing the atomization process, numerical simulations have been widely used in the past [15-19]. However, a detailed resolution of the entire atomization process till the smallest droplets requires extremely high computational resources. Therefore, numerical investigations on atomization consider generally the primary breakup process of the intact liquid core and the dispersion of small-scale droplets in the secondary breakup process separately [20-23]. For instance, a common approach for modeling spray dispersion is given by the hybrid Eulerian-Lagrangian method, which introduces a number of Lagrangian parcels with pre-defined sizes and velocities for representing droplets within the spray, which are injected from given inlet positions close to the atomizer and tracked during the simulation. However, the assumptions made by this concept are mostly different from the real primary breakup physics and the accuracy of the simulation relies upon a number of tuning parameters, which need to be determined based on limited measurement data or even completely arbitrarily. Accordingly, models for capturing the primary breakup behavior are necessary to understand the physical mechanism behind and to achieve more accurate modeling of the spray.

For that reason, high-fidelity numerical simulations have been conducted in this work for a twin-fluid, coaxial nozzle. The nozzle has been designed, built and experimentally investigated in the framework of the bioliq® process for EFG of high viscous biomass slurry fuel [24], which aims to convert biogenic residues into high quality syngas or chemicals. Objective of the current work is to reveal specifically the influence of the relative injection angle between the central liquid jet and the annular gaseous coflow on breakup of the liquid jet. The simulation results are validated by means of

corresponding experimental data and used to derive correlations of important breakup characteristics, such as the breakup length, with the relative injection angle [24].

Experimental Conditions

The simulations have been conducted for a generic atomization test rig, which is specifically designed for studying atomization process of high viscous liquids in EFG application [05]. It consists of a twin-fluid nozzle and an optically accessible reactor chamber. The generic design of the system allows the investigation of specific parameters influencing spray quality, such as the fluid viscosity or nozzle design parameters on the atomization process. For the current study, a glycerol/water mixture (glycerol in wt. 89.5%) was atomized at atmospheric condition with a temperature of 293 K and an ambient pressure of 1 bar. The mass flow rate of liquid from the central liquid tube is 20 kg/h and that of the annular airflow is 12 kg/h, leading to a gas-to-liquid mass flow ratio of *GLR*=0.6. The gas-to-liquid injection angle α between liquid and air flows has been varied from $\alpha = 0°$ to 30° in the experiment, and α has been varied up to 60° for the numerical simulation. Figure 1 shows the geometrical dimensions of the used nozzle system with different α. For all nozzles, the diameters of the liquid and gas nozzles at the exit plane are kept constant at d_L = 2 mm and d_G = 7.96 mm. The web thickness connecting the external wall of the liquid tube and inner wall of the gas nozzle is *b*=0.1 mm.

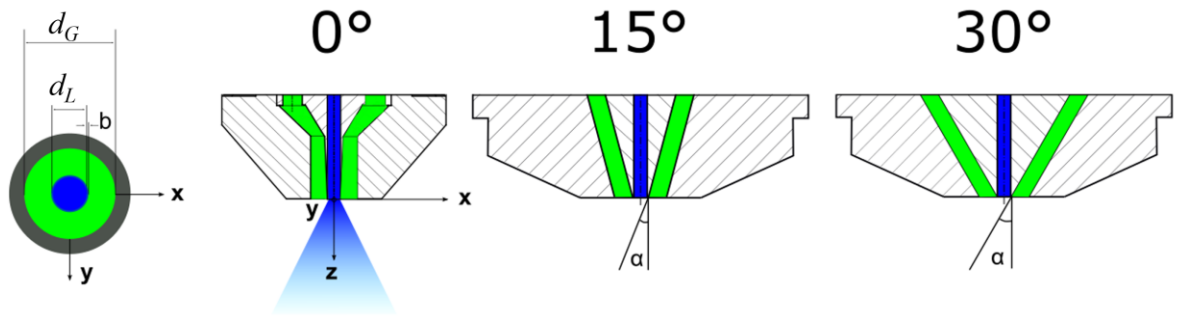

Figure 1: Geometries of the used twin-fluid nozzles with different gas-to-liquid injection angles.

Table 1 summarizes the characteristic dimensionless parameters, with the liquid Reynolds number Re_L, the gaseous Reynolds number Re_G, the momentum ratio *MR*, the momentum flux ratio *M*, the aerodynamic Weber number We_{aero} and the Ohnesorge number Oh. These non-dimensional parameters are calculated with

$$Re_L = \frac{u_L d_L}{\nu_L}, Re_G = \frac{u_G d_{Gap}}{\nu_G}, MR = \frac{\rho_G u_G^2 A_G}{\rho_L u_L^2 A_L}, M = \frac{\rho_G u_G^2}{\rho_L u_L^2}, We_{aero} = \frac{\rho_G u_R^2 d_L}{\sigma}, Oh = \frac{\mu_L}{\sqrt{\rho_L \sigma d_L}} \quad (1)$$

where $u_L = 1.446$ m/s and $u_G = 61.356$ m/s are the bulk flow velocities issuing from the liquid and gas nozzles, $u_R = u_G - u_L$ the relative velocity between both streams; $d_{Gap} = d_G - d_L - b$ the gap distance of the annular gas flow. A_L and A_G are the cross-section area of the liquid and gas nozzles at the exit plane. The glycerol/water mixture is a Newtonian fluid, which has a dynamic viscosity of μ_L=200 mPa·s and a density of ρ_L=1223 kg/m^3. The surface tension of liquid is set to $\sigma = 6.4$ mN/m. The viscosity and density of air are equal to μ_G=0.0185 mPa·s and ρ_G=1.182 kg/m^3. In the current study, the non-dimensional parameters remain constant while varying α. The readers are referred to [05] for a more detailed description of the nozzle system.

Table 1. Characteristic dimensionless parameters for primary atomization of coaxial glycerol/water jet.

α	Re_L	Re_G	*MR*	*M*	We_{aero}	*Oh*
0 – 60°	18	22,600	25.7	1.8	132	0.5

Figure.2 shows snapshots from high speed imaging of the liquid jet at different gas-to-liquid injection angles. In all cases, the liquid jet is disturbed by the surrounding high-speed airflow, which leads to formation of wavy pattern on the liquid column and a flapping motion of the central jet around the symmetry axis. Thereafter, membrane-like thin sheets pinch off from the tip of the liquid jet, which break up further into smaller droplets. The breakup morphology is characterized as membrane-type breakup, which is classified for relatively high Re_L and low We_{aero} in the range of $25<We_{aero}<70$ and

Re_L>200 for coaxial water jets in [08]. However, the current work applies a high-viscous glycerol-water mixture with 200 mPa·s, which is 200 times larger than the viscosity of water. This leads to a considerably lower Re_L (see Tab.1) compared with those of water jets used for classifications of breakup regimes. Therefore, the breakup morphology in the current work is given by the membrane-type regime, although We_{aero} is larger than 70. For α = 15° a stabilizing region along the liquid jet is detected. A further increase in gas jet angle from α = 15° to 30° leads to a decrease in the length of the aforementioned stabilization region. The length of this less disturbed jet is dependent on the impact area, given by the projection area of the tilted coaxial gas flow onto the central liquid jet core, which decreases with α.

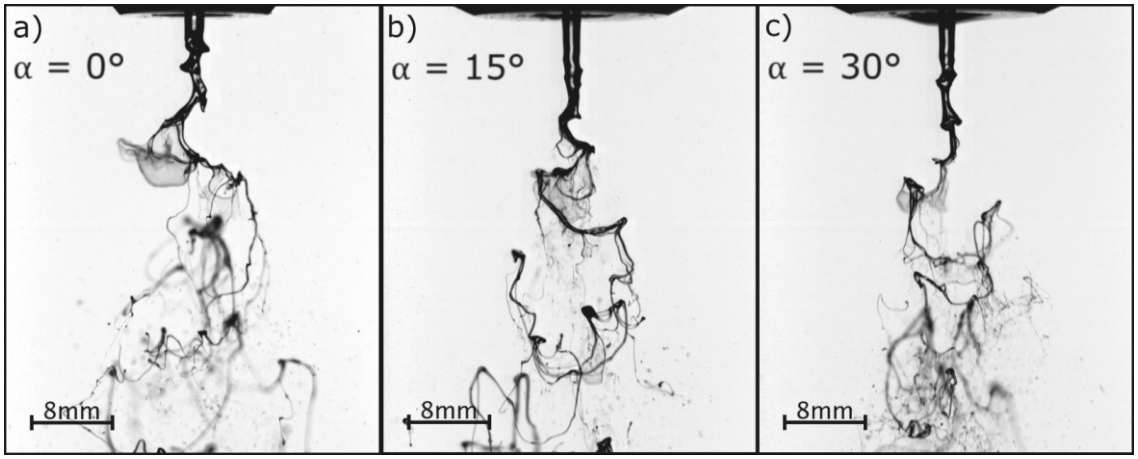

Figure 2: Snapshots from high-speed imaging of primary atomization of coaxial liquid jet at different relative air-to-liquid injection angles.

Figure 3 compares contour plots of time-mean streamwise velocity $\bar{u}$ [m/s] obtained from particle image velocimetry (PIV) measurement for the cases with α=0° and α=30°. As the liquid jet reflects the high-intensity laser beam, it is difficult to measure the gas phase flow velocity together with the liquid phase. Therefore, a solid cylindrical pin (blanked fields in Fig.3) with a diameter of 2 mm and a length of 10 mm is mounted at the exit of the liquid nozzle, which is used to represent the intact liquid jet core. As a consequence, the measured velocity distributions in Fig.3 are shown only for one side of the pin, whereas the other half lies on the shadow side of the pin and cannot be illuminated by the laser beam. It can be seen from Fig.3 that an increase of α from 0° to 30° results in an increased streamwise velocity. While the high-speed airflow hits the pin at an increased α, a stagnation point with increased static pressure is induced at the base of the pin. This leads to a favorable pressure gradient along the streamwise direction and an acceleration of the surrounding gas flow at increased α. The behavior has been confirmed in the following by results from the numerical simulations (see Fig.7 and Fig.8).

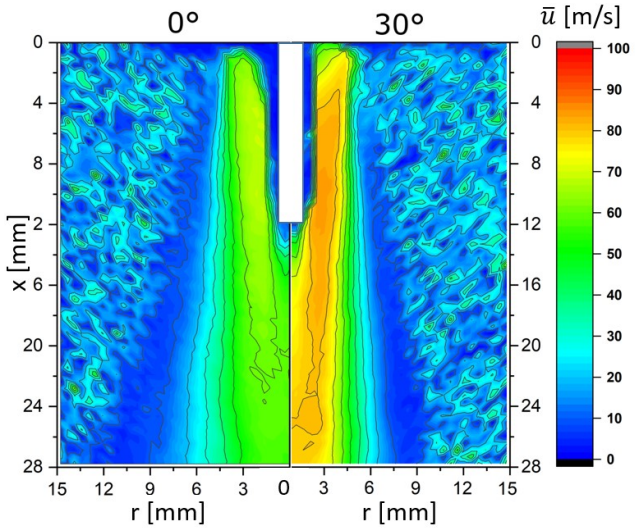

Figure 3: Comparison of measured time-mean streamwise velocities for α=0° and α=30°.

Simulation Setups

Figure 4 on the left depicts a cutting plane of the 3D computational domain through the centerline axis, where d_L represents the diameter of the liquid nozzle at the exit plane. The relative injection angle α between liquid and air streams is indicated in Fig.4 in the top-right corner. The cone-shaped computational domain has a length of $30d_L$ in streamwise direction, with the diameters of $10d_L$ and $20d_L$ at the inlet and at the outlet of the domain, as indicted in Fig.4 on the left. The domain starts directly at the nozzle exit plane and covers the entire range of primary atomization. The internal geometries of the nozzle for different α have not be considered in order to use the same computational grid for different α cases. This allows a better evaluation regarding specifically the effect of α, excluding the influence of different nozzle interior geometries. The dimensions of the domain have been selected based on a compromise between simulation accuracy and computational cost; it allows use of refined grid resolutions in the near field with the liquid jet and the outlet plane lies sufficiently far away from the jet core, so that "zero gradient" type boundary condition can be fairly applied. The entrainment boundary on the side allows entering of ambient air into the domain. The x-axis indicates the streamwise direction and the origin of the axes is located at the center of the liquid inlet.

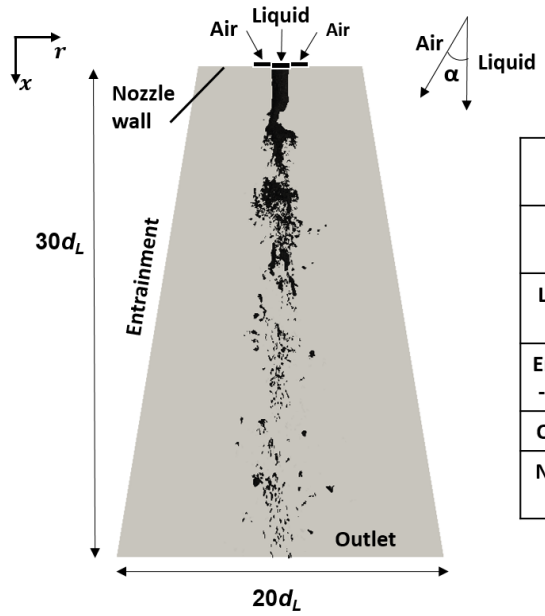

BC	Velocity	Temperat.	Liquid vol. fraction [-]
Air inlet	$\dot{m}_{Gas}$= 12 kg/h	T= 293 K	f=0
Liquid inlet	$\dot{m}_{liquid}$= 20 kg/h	T= 293 K	f=1
Entrain -ment	$\nabla u = 0$	∇T=0	∇f=0
Outlet	$\nabla u = 0$	∇T=0	∇f=0
Nozzle wall	$u = 0$ m/s	∇T=0	f=0

Figure 4: Computational domain (left) and list of boundary conditions (right).

The computational grid consists of 9.5 million hexahedral elements, which are locally refined close to the liquid jet. It has a smallest resolution of $\Delta_{min,r}$=25 µm in the radial direction and the grid length in the streamwise directions starts with the smallest resolution of $\Delta_{min,x}$=50 µm. The grid size expands with a small ratio in radial and streamwise directions. A meridian cut-plane through the computational grid is shown in Fig.5, along with contours of instantaneous volume fraction of liquid f. It can be seen that the gas-liquid interface represented by the sharp gradient of f is resolved adequately by 2 – 3 cells. Nonetheless, the resolution used is not sufficient to resolve the small-scale droplets downstream. Therefore, focus of this work is to study the destabilization and breakup processes of the liquid jet core, along with pinch-off of primary large liquid ligaments from the core jet.

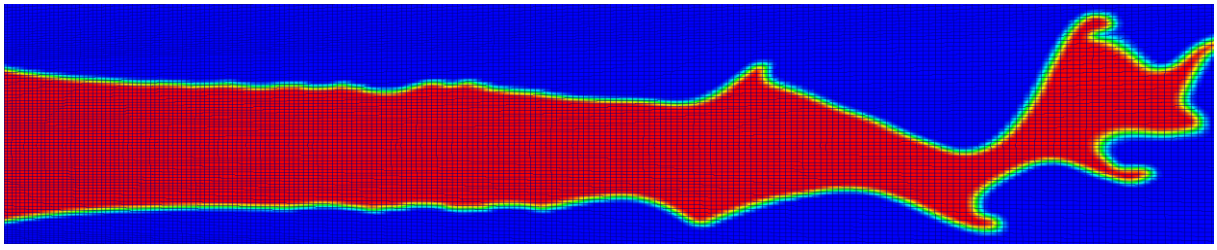

Figure 5: Instantaneous volume fraction of liquid on a cutting plane passing through the centerline axis; the grid lines are shown in order to illustrate the grid resolution.

The open-source code OpenFOAM [25] has been used to perform the numerical simulations and the standard solver "compressibleInterFoam" from OpenFOAM is selected to simulate the turbulent multiphase flow. The gas-liquid interface is captured by means of the volume of fluid (VOF) method [26, 27], where the liquid and gas phases are treated as one fluid and a balance equation is solved for the volume fraction of liquid *f*, in addition to the continuity and momentum equations. The material properties of the virtual "mixture" fluid with both liquid and gas phases, such as the density and the viscosity, are calculated based on the volume-weighted average by means of *f*. The VOF method represents state-of-the-art technique for modeling multiphase flows and has already been extensively validated in previous works [15, 16, 17, 18, 19, 28, 29]. A detailed description of the VOF method as well as its implementation in OpenFOAM can be found in [18, 26].

The boundary conditions used for solving the balance equations are given in Fig.4 on the right. There, the flow velocities entering the gas and liquid inlets were set according to the given mass flow rates by experiment and no-slip condition was used for the nozzle walls. The temperature was prescribed at 293 K at the inlets, and *f* was equal to zero at the gas inlet and 1 at the liquid inlet. At the entrainment and outlet boundaries, gradients of the transport variables were set to zero. The balance equations have been solved in a fully compressible formulation, employing 2nd order schemes for discretization of the convective and diffusive terms. The time step is set to Δt=0.2 µs, which leads to a maximum CFL number of 0.5. Statistical averaging of the flow has been performed for a physical time of 80 ms or 400,000 time steps, which corresponds to more than 10 flow-through times based on the bulk velocity of liquid stream and the primary breakup length. The turbulent flow is modeled in this work with the large eddy simulation (LES) technique, which is able to resolve directly the large-scale flow structures on the grid. The wall-adapted local eddy viscosity (WALE) model has been applied for the sub grid Reynolds stresses, considering the effect of unresolved turbulent fluctuations.

Simulation Results

- **Breakup Mechanism**

Figure 6 shows contours of instantaneous velocity in the main flow direction on a meridian cut-plane for different relative injection angles, where the liquid jet core is depicted by the iso-contours of liquid volume fraction with *f*=0.5. In all cases with different α, the gas phase flow velocity represented by the region outside the solid line is much higher compared with that of the liquid phase (enclosed by the solid line). An inner shear layer with large velocity gradient between the high-speed annular airflow and low-speed liquid jet, as well as an outer shear layer between the airflow from the nozzle and the ambience can be detected, which leads to formation of coherent vortices at these shear layers and generation of small-scale waves along the liquid jet surface. These flow instabilities grow further downstream and disturb the liquid jet through aerodynamic force or exchange of momentum, respectively.

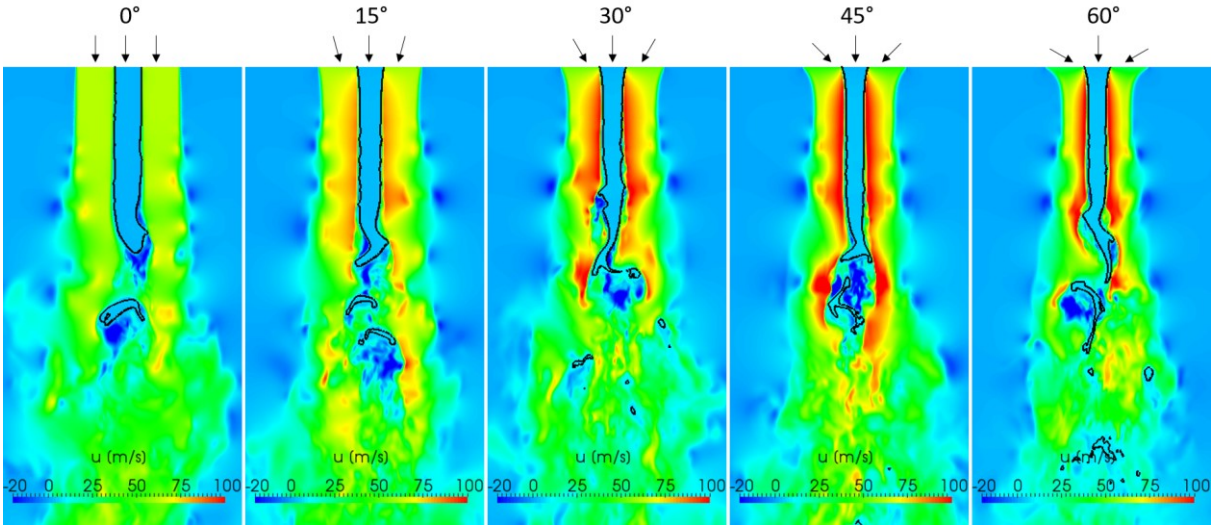

Figure 6: Contours of instantaneous streamwise velocity calculated from VOF-LES simulations of primary breakup of coaxial glycerol/water jet at different air-to-liquid injection angles.

In addition, the impact area, given by the projection area of the air flow direction onto the liquid column, decreases and the radial velocity component of the gas stream increases with α, which promotes destabilization of the liquid jet. As a consequence, the overall momentum transfer from the gas to the liquid phase is increased with α. At the tip of the liquid jet, large-scale, concentric vortices followed from the initial flow disturbances penetrate into the liquid jet, where the recirculating flow from both sides of the jet results in thinning of the liquid core. At the same time, the tip of the liquid jet is accelerated toward streamwise direction and oscillates around the centerline axis due to interference caused by the turbulent vortices, until first liquid ligaments disintegrate from the jet. This breakup mechanism is representative for all cases with different α.

Figure 7 shows contours of the time-averaged streamwise velocity on the same meridian cut-plane, where the liquid jet core is depicted by the iso-surface of the time-mean liquid volume fraction at $\bar{f} = 0.5$. The length of the liquid jet core L_C, determined with the largest axial distance of the $\bar{f} = 0.5$ iso-surface, decreases with the injection angle until α=30°, and then increases again with α from 30° to 60°. This behavior can be explained with the increased streamwise velocity of airflow close to the gas-liquid interface, as depicted in Fig.6 and Fig.7. As the high-speed airflow hits the liquid column, the gas flow velocity decreases to adapt to the low-speed liquid jet. In particular, the radial motion of the gas is forced to be stalled at the surface of liquid jet. As a consequence, one part of the kinetic energy of the airflow is converted to pressure energy while hitting the liquid jet at increased α. This generates a stagnation point with increased static pressure at the base of the liquid jet (see Fig.8).

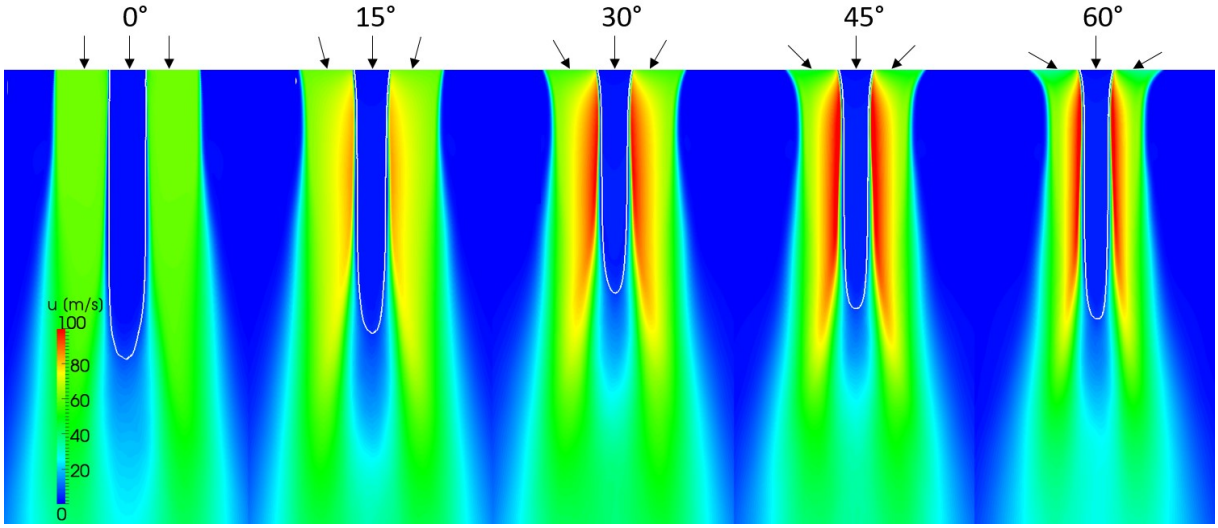

Figure 7: Contours of time-mean streamwise velocities calculated from VOF-LES simulations of primary breakup of coaxial glycerol/water jet at different air-to-liquid injection angles.

The local high pressure near the base of the liquid jet results in a favorable pressure gradient and an acceleration of the airflow along the gas-liquid interface and towards the streamwise direction, so that the velocity of gas flow increases with α up to α=30°. The same result has been confirmed by PIV measurement, as shown in Fig.3. The increased gas flow velocity results in an increased gradient of the flow velocity at the gas-liquid interface, so that the aerodynamic force exerted on the liquid jet or the momentum transfer from the gas to the liquid is reinforced. For this reason, the liquid jet breaks faster or the breakup length decreases with α in this case.

Figure 8 illustrates contours of the time-mean static pressure $\bar{p}$, where the jet core is depicted by the iso-contours of $\bar{f} = 0.5$. The pressure near the base of liquid jet increases with α until α=45°, which leads to an increased streamwise velocity of the airflow, as shown in Fig.6 and Fig.7. However, further increase of α from 45° to 60° does not lead to an increased gas phase static pressure at the stagnation point, so that the peak values of streamwise velocity decreases and L_C increases with α in this case. Similar behavior has been found for the calculated root-mean-square values of the turbulent fluctuations, which increase from α=0° to 45° and decreases again with further increased α.

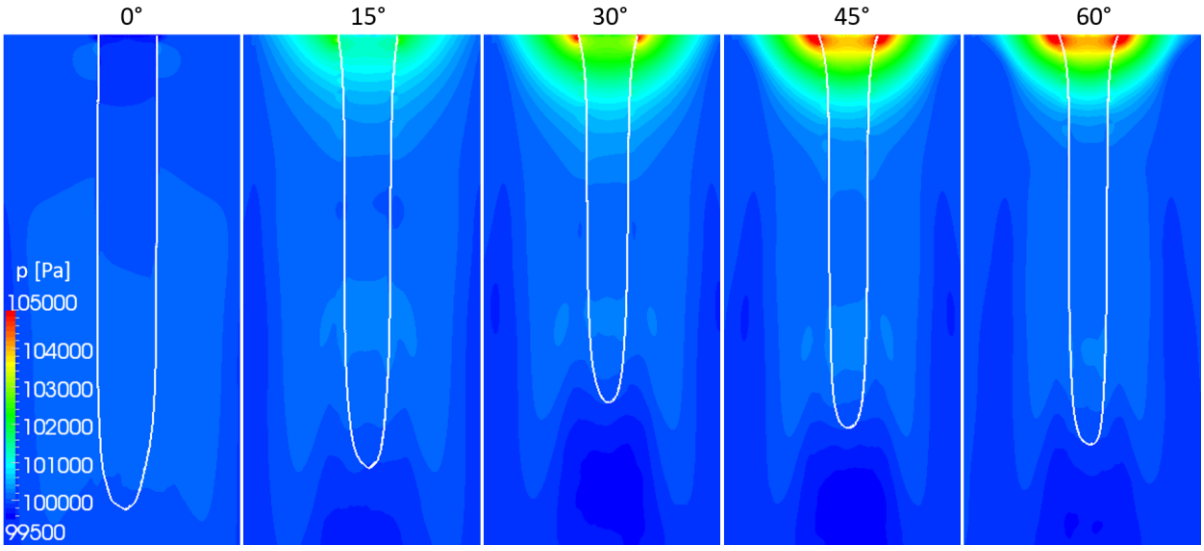

Figure 8: Contour-plots of time-mean static pressure calculated from VOF-LES of primary breakup of coaxial glycerol/water jet at different air-to-liquid injection angles.

- **Breakup Length**

Figure 9 on the left shows profiles of the time-mean (solid lines for $\bar{f}$) and root mean square values (dashed lines for f_{rms}) of the liquid volume fraction along the centerline axis. Throughout the breakup process, $\bar{f}$ decreases from 1 to 0 along the streamwise axis. In the range of α<30°, $\bar{f}$ decreases faster with increased α, confirming a reduction of the breakup length L_C with α. However, $\bar{f}$ yields a slowed decrease along the x-axis while α rises from 30° to 60°, revealing again an increase of L_C. The modification of L_C with α can also be perceived in Fig.8 by means of iso-contours of $\bar{f} = 0.5$, as well as from the streamwise profiles of f_{rms}, where the maximum value of f_{rms} with $f_{rms,max} \approx 0.5$ shifts with varied α. The location of $f_{rms,max}$ (corresponding to $\bar{f} \approx 0.5$) has been used to identify the breakup length L_C from the simulations [19], which is shown in Fig.9 on the right against α. The predicted L_C decreases from α=0° to α=30° and it increases again from α=30° to α=60°, indicating a most effective atomization in the range of 30°<α<45°.

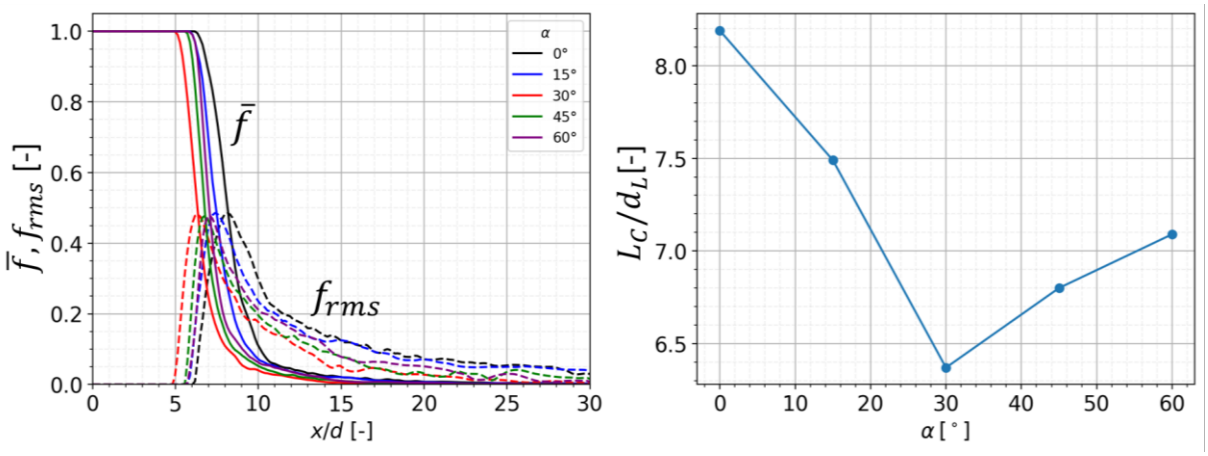

Figure 9: Profiles of time-mean and rms values of liquid volume fraction along the centerline axis for different relative air-to-liquid injection angles α (left) and progresses of calculated breakup length L_C from $f_{rms,max}$ in dependence of α (right).

Conclusion

High-fidelity numerical simulations have been carried out to study the primary atomization process of a coaxial glycerol/water jet under atmospheric condition. The objective is to gain an in-depth understanding of the effect of varied air-to-liquid injection angles α on the breakup behavior. The simulation results have shown a good agreement with corresponding experiment, revealing a pulsating

mode instability of the liquid jet, along with disintegrations of membrane-type liquid ligaments. An increase of α from 0° to 30° leads to a contracted liquid core and a shorter liquid core length. The reason is attributed to an increased gas phase flow velocity on the liquid surface, which leads to a reinforced aerodynamic force or multiphase momentum exchange. However, the reversed effect is found for further increased α from 30° to 60°, where the breakup length increases and the calculated kinetic energy of liquid phase decreases with increased α, yielding an attenuated momentum transfer from the gas to the liquid phase. In conclusion, the geometrical design parameter of the nozzle, such as the relative injection angle studied in this work, has an essential impact on the atomization behavior, which should be taken into account, in addition to the general operating parameters such as the Reynolds number, the Weber number or the momentum flux ratio.

Acknowledgments

The authors gratefully acknowledge the financial support by the Helmholtz Association of German Research Centers (HGF), within the research field MTET (Materials and Technologies for the Energy Transition), subtopic "Anthropogenic Carbon Cycle" (38.05.01). This work utilized computing resources provided by the High Performance Computing Center Stuttgart (HLRS) at the University of Stuttgart and the Steinbuch Centre for Computing (SCC) at the Karlsruhe Institute of Technology.

References

[01] Higman C., Burgt M.: Gasification. 2nd edition, Gulf Professional Publishing, 2008.
[02] Kolb T., Aigner M., Kneer R., Müller M., Weber R., Djordjevic N.: Tackling the challenges in modelling entrained-flow gasification of low-grade feedstock, J. Energy Inst., 89(4), 485-503, 2016.
[03] Svoboda K., Pohorely M., Hartman M., Martinec J.: Pretreatment and feeding of biomass for pressurized entrained flow gasification, Fuel Process. Technol. 90, 629-635, 2009.
[04] Jakobs T., Djordjevic N., Fleck S., Mancini M., Weber R., Kolb T.: Gasification of high viscous slurry R&D on atomization and numerical simulation. Applied energy 93, 449-456, 2012.
[05] Wachter S, Jakobs T, Kolb T: Experimental investigation on the influence of system pressure on resulting spray quality and jet breakup applying pressure adapted twin-fluid nozzles. Int J Multiph Flow 125, 2020.
[06] Dumouchel C.: On the experimental investigation on primary atomization of liquid streams, Exp. Fluids, 45(3) 371-422, 2008.
[07] Eroglu H., Chigier N., Farago Z.: Coaxial atomizer liquid intact lengths. Phys Fluids A 3(2), 303-308, 1991.
[08] Farago Z., Chigier N.: Morphological classification of disintegration of round liquid jets in a coaxial air stream, At. Sprays 2(2) 137-153, 1992.
[09] Woodward R., Burch R., Kuo K.K., Cheung F.B.: Correlation of intact-liquid core length for coaxial injectors. In: Proceedings of ICLASS, Vol. 94, 105-112, 1994.
[10] Engelbert C., Hardalupas Y., Whitelaw J.H. Breakup phenomena in coaxial airblast atomizers. Proc R Soc London A. 451, 189-229, 1995.
[11] Lasheras J., Villermaux E., Hopfinger E.: Break-up and atomization of a round water jet by a high-speed annular air jet. J Fluid Mech 357, 351-379, 1998.
[12] Lasheras J.C., Hopfinger E.: Liquid jet instability and atomization in a coaxial gas stream. Annu Rev Fluid Mech 32(1), 275-308, 2000.
[13] Shavit U.: Gas-liquid interaction in the liquid breakup region of twin-fluid atomization. Exp Fluids 31(5) 550:7, 2001.
[14] Mayer W.O.H., Branam R.: Atomization characteristics on the surface of a round liquid jet, Exp. Fluids 36, 528-539, 2004.
[15] Shinjo J., Umemura A.: Simulation of liquid jet primary breakup: Dynamics of ligament and droplet formation, Int. J. Multiph. Flow 36, 513-532, 2010.
[16] Xiao F., Dianat M., McGuirk J.J.: LES of turbulent liquid jet primary breakup in turbulent coaxial air flow, Int. J. Multiph. Flow 60, 103–118, 2014.
[17] Tian X., Zhao H., Liu H., Li W., Xu J.: Three-dimensional large eddy simulation of round liquid jet primary breakup in coaxial gas flow using the VOF method, Fuel Process. Technol. 131, 396–402, 2015.

[18] Müller T., Sänger A., Habisreuther P., Jakobs T., Trimis D., Kolb T., Zarzalis N.: Simulation of the primary breakup of a high-viscosity liquid jet by a coaxial annular gas flow, Int. J. Multiph. Flow 87, 212-228, 2016.
[19] Zhang F., Zirwes T., Müller T., Wachter S., Jakobs T., Habisreuther P., Zarzalis N., Trimis D., Kolb T.: Effect of elevated pressure on air-assisted primary atomization of coaxial liquid jets: basic research for entrained flow gasification. Renew. Sustain. Energy Rev. 134, 110411 2020.
[20] Saeedipour M., Pirker S., Bozorgi S., Schneiderbauer S.: An Eulerian-Lagrangian hybrid model for the coarse-grid simulation of turbulent liquid jet breakup, Int. J. Multiph. Flow 82, 17–26, 2016.
[21] Béard P., Duclos J.M., Habchi C., Bruneaux G., Mokaddem K., Baritaud T.: Extension of Lagrangian-Eulerian Spray Modeling: Application to High Pressure Evaporating Diesel Sprays, SAE Trans. 109, 1417-1434, 2000.
[22] Subramaniam S.: Lagrangiane Eulerian methods for multiphase flows, Prog. Energy Combust. Sci 39, 215-245, 2013.
[23] Zhang F., Heidarifatasmi H., Harth S., Zirwes T., Wang R., Fedoryk M., Sebbar N., Habisreuther P., Trimis D., Bockhorn H.: Numerical evaluation of a novel double-concentric swirl burner for sulfur combustion. Renewable and Sustainable Energy Reviews, 133, 110257, 2020.
[24] Wachter S., Jakobs T., Kolb T.: Towards system pressure scaling of gas assisted coaxial burner nozzles - An empirical model. Applications in Energy and Combustion Science 5, 2021.
[25] Fleck S., Santo U., Hotz C., Jakobs T., Eckel G., Mancini M., Weber R., Kolb T.: Entrained flow gasification Part 1: Gasification of glycol in an atmospheric-pressure experimental rig. Fuel 217, 306-319.
[26] Prosperetti A., Tryggvason G.: Computational Methods for Multiphase Flow, Cambridge University Press, 2009.
[27] Yeoh G.H., Tu J.: Computational Techniques for Multiphase Flows, 2nd Edition, Butterworth-Heinemann, 2019.
[28] Saito K., Srinivasan V., Salazar A.J.: Modeling the disintegration of modulated liquid jets using volume-of-fluid methodology, Appl. Math. Modell 35, 3710–3730, 2011.
[29] Grosshans H., Movaghar A., Cao L., Oevermann M., Szász R.Z., Fuchs L.: Sensitivity of VOF simulations of the liquid jet breakup to physical and numerical parameters, Comput. Fluids 136, 312–323, 2016.